Measurement of GPS Antenna Gain Patterns for CYGNSS using a Spaceborne Antenna Range

Tianlin Wang, Member, IEEE
The Ohio State University, Columbus, OH 43210, USA

Christopher S. Ruf, Life Fellow, IEEE
University of Michigan, Ann Arbor, MI 48109, USA

Andrew J. O'Brien

Scott Gleason, Senior Member, IEEE
Daaxa LLC, Boulder, CO 80305, USA

Darren S. McKague, Member, IEEE
University of Michigan, Ann Arbor, MI 48109, USA

Bruce P. Block
University of Michigan, Ann Arbor, MI 48109, USA

Anthony Russel
University of Michigan, Ann Arbor, MI 48109, USA

Manuscript received 21 April 2023; revised 14 December 2023 and 23 May 2024; accepted 28 May 2024.

DOI. No. XXXXX XXXXX

This work was supported in part by NASA Science Mission Directorate contract NNL13AQ00C with the University of Michigan.

Authors' addresses: Tianlin Wang is with the Department of Electrical and Computer Engineering and ElectroScience Laboratory, The Ohio State University, Columbus, OH 43210, USA, E-mail: (wang.15085@osu.edu); Christopher S. Ruf is with the Department of Climate and Space Sciences and Engineering, University of Michigan, Ann Arbor, MI 48109, USA, E-mail: (cruf@umich.edu); Andrew J. O'Brien, E-mail: (andrew.obrien.200@gmail.com); Scott Gleason is with Daaxa LLC, Boulder, CO 80305, USA, Email: (sgleason@protonmail.com); D. S. McKague is with Department of Climate and Space Sciences and Engineering, University of Michigan, Ann Arbor, MI 48109, USA, Email: (dmckague@umich.edu); Bruce P. Block and Anthony Russel are with the Space Physics Research Laboratory, University of Michigan, Ann Arbor, MI 48109, USA, Email: (bpblock@umich.edu; russelan@umich.edu).

(*Corresponding author: Tianlin Wang*.)

***Abstract*—**The NASA CYGNSS mission is a constellation of 8 small satellites that receive GPS signals reflected off the Earth to support a variety of science applications. For remote sensing, the strength of the reflected GPS signal contains important information and must be known to a small fraction of a dB. This makes it very different than traditional GPS navigation applications in which small amplitude variations have minor or negligible impact depending on the accuracy requirements of the specific application. Satisfying mission requirements necessitates precise knowledge of the GPS satellite transmit antenna pattern and the receive antenna pattern on each CYGNSS satellite. In this paper, we present the antenna calibration approach that is used by the CYGNSS science operations center. GPS satellite and CYGNSS satellite antenna patterns are jointly estimated using several years of on-orbit CYGNSS measurements. The orbiting GPS transmit and CYGNSS receive antennas form a spaceborne antenna measurement range which can be utilized to determine their patterns. The accuracy of the estimated antenna patterns can then be quantified using CYGNSS GPS science data as a metric. When compared to the limited publicly-available GPS satellite antenna data or antenna chamber measurements of the CYGNSS satellites, the proposed on-orbit approach is able to introduce corrections that significantly improve the CYGNSS mission science performance.

I. INTRODUCTION

Global navigation satellite system (GNSS) is the generic term used for constellations of navigation satellites that provide positioning, navigation, and timing (PNT) services on a global basis. GNSS is currently used in many applications including navigation, surveying, mapping, and remote sensing [1] [2]. Each GNSS satellite continuously transmits radio frequency (RF) signals towards the Earth, which propagates and is then captured by the receiver system, which could be either ground-based, airborne or spaceborne. The power level of received GNSS signals on the Earth is extremely low, typically -160 dBW (decibel-watts) for the Global Positioning System (GPS). The signal structure allows a receiver to extract the signal buried in background RF noise and make precise PNT measurements [2]. The GPS satellite transmit antenna is designed to be right-hand circular polarized (RHCP), although the polarization purity of the pattern has not been made publicly available nor published in open literature.

GNSS-reflectometry (GNSS-R) uses reflected GNSS signals for Earth remote sensing applications [3] [4]. Calibration of its Delay Doppler Map (DDM)

measurements of surface scattering cross section requires knowledge of the effective isotropic radiated power (EIRP) of the GNSS transmitter, e.g. GPS [5]. This in turn requires knowledge of the GPS transmit power level and the GPS transmit antenna gain pattern. For the NASA Cyclone Global Navigation Satellite System (CYGNSS) GNSS-R mission [6] [7], DDM calibration is accomplished by its Level 1 calibration algorithm [8], [9]. Changes in GPS transmit power are tracked by real time monitoring of the power level of direct signals received by the navigation receiver on each CYGNSS spacecraft [10] [11]. The GPS transmit antenna pattern can also be determined from the same direct signals. Additionally, the direct signal measurements allow for determination of the receive antenna patterns on each CYGNSS spacecraft. The work presented here describes how both patterns are derived from a large collection of direct signal measurements made by the constellation of CYGNSS spacecraft.

The first published GPS L-band RHCP antenna patterns included four azimuthal cuts of the relative gain from a Block IIA antenna [12]. Measurements from the Radio Amateur Satellite Corporation (AMSAT) experiment showed that the main lobes on the Block IIR satellites were slightly narrower than the Block II/IIA patterns and that some side-lobe levels for Block IIR satellites were significantly higher than expected [13]. This demonstrated that the gain pattern could be significantly affected by the space vehicle (SV) on which it was mounted. Over the next 2 decades, the publicly available GPS antenna patterns are the measurements for satellites collected during prelaunch testing and published on the GPS Technical References website [14]. However, these patterns either only have coarse resolution (2 degree in off-boresight, and 10 degrees in azimuth), or only include an azimuthally averaged cut, instead of the full antenna pattern. The published patterns by Lockheed Martin [15] have been used to determine the transmit power of GPS satellites in various ground-based experiments [16]–[18]. Note that cross-polarization information is not provided in these published patterns, which were assumed to be purely RHCP. Azimuthal asymmetry in the patterns has been observed by these experiments. Additional studies have shown that the published pre-launch patterns are not of sufficient accuracy to meet the requirements of some GNSS-R scientific investigations [19].

On orbit determination of GPS transmit antenna gain patterns was attempted previously by the GPS Antenna Characterization Experiment (ACE), a research collaboration between the Aerospace Corporation and NASA Goddard Space Flight Center (GSFC). GPS ACE characterized the side-lobe portion of GPS L1 antenna patterns using receivers in a geosynchronous equatorial orbit (GEO) [20]. Notably, the main beam (on-Earth) portion of the GPS antenna pattern was not characterized, and the patterns were assumed to be purely RHCP.

The work presented here expands upon the approach initially developed by GPS ACE using GPS receivers deployed on the constellation of CYGNSS satellites in Low Earth Orbit (LEO), rather than in GEO. This measurement geometry allows for sampling of the transmitted signal throughout the main beam portion of the GPS antenna pattern. Like the previous work mentioned above, the GPS satellite transmit pattern has been reasonably assumed to be pure RHCP, and we expect to be measuring the RHCP component of the CYGNSS receive GPS antenna. The link equation for the received signal power is inverted to determine the receive antenna pattern on each CYGNSS satellite. Additionally, the GPS transmit antenna gain pattern can also be determined by inversion of the link equation. The retrieval procedure, validation with pre-launch chamber measurements, and impact on CYGNSS Level 1 calibration are detailed in the following sections.

Portions of this article appeared previously in the first author's Ph.D. thesis [21].

II. SPACEBORNE ANTENNA RANGE MEASUREMENTS

A. Constellations of GPS and CYGNSS

The GPS constellation of satellites are all in Medium Earth Orbit (MEO) at 20,180 km altitude. There are currently 31 operational satellites consisting of 4 different SV designs (referred to as block types), including Block IIR, IIR-M, IIF, and III. For Block IIR and IIR-M SVs, there are two antenna designs used.

The CYGNSS constellation of 8 satellites are all in LEO at 520 km altitude. They share a common orbit plane, and the orbit period is approximately 95 minutes. Each spacecraft carries a navigation receiver connected to a zenith-mounted antenna that receives direct GPS L1 C/A (coarse/acquisition) code signals for navigation. Two science receivers connected to nadir-mounted antennas also receive reflected GPS signals from the Earth surface for remote sensing applications. While calibration of these nadir GPS antennas is important for a number of science applications, it is not the focus of this work.

TABLE I
GPS AND CYGNSS CONSTELLATION

Cons.	GPS	CYGNSS
Orbit	MEO	LEO
Height (km)	20,180	~ 520
Inclination (º)	55	35
Period	11 hours 58 minutes	~ 95 minutes
# of satellites	31 active	8
Block Type	IIR, IIR-M, IIF, III	Uniform

The CYGNSS zenith navigation antenna is a half-wave dipole patch. Its gain pattern was measured in an anechoic chamber prior to launch while mounted on a satellite mock-

up. Those measurements revealed that the pattern is affected by coupling and multipath from nearby structures on the spacecraft. The measured pattern cannot be assumed to be an accurate representation of the on-orbit patterns owing to mechanical tolerances and limits on repeatability that are associated with final assembly of the spacecraft. For these reasons, the on-orbits patterns may differ from the pre-launch pattern and from one another.

Examples of the GPS transmit antenna (Block IIR, legacy antenna panel) and CYGNSS zenith antenna are shown in Fig. 1(a) and 1(b), respectively.

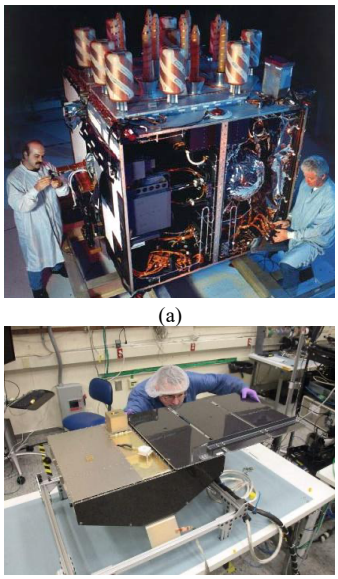

(a)

(b)

Fig. 1. Example photos of the antennas being measured in this work, where (a) shows GPS transmit antenna (Block IIR) [15] and (b) shows CYGNSS zenith GPS receive antenna (white square radome) during satellite assembly

B. Spaceborne Antenna Measurement Range

CYGNSS provides a unique opportunity for precise determination of the GPS transmit and CYGNSS receive antenna gain patterns which includes the effects of satellite structures on their patterns. Both the GPS and CYGNSS satellites have precisely known positions and orientations, they are in orbit well above any tropospheric propagation effects, and they are free of environmental multipath. At these altitudes, the only propagation effect that could potentially impact the measurement is ionospheric scintillation. When GPS receivers are used in low-Earth orbit (LEO), ionospheric effects must still be considered since, although scintillation tends to be generated at the maximum electron density at approximately 350 km where irregularities occur, the ionosphere extends from 50 km to more than 1000 km [22]. Models, such as the global ionospheric scintillation model can be used to estimate the scintillation index (S4) and predict the degradation of the amplitude of the received GPS signal. In [22], an example of ionospheric impact is characterized on a receiver in typical LEO orbit, showing that about 60% of the TEC is above the receiver, and the depth of the scintillation fading ranges from 2 to more than 20 dB, depending on the solar activity. Nonetheless, these ionospheric events are expected to be rare and the results here are aggregated over several years of measurements. The method of analysis used effectively averages the ionospheric effects over this time period.

In this sense, measurements between the two satellites form an ideal "spaceborne antenna range". It provides a unique opportunity for precise determination of the GPS transmit and CYGNSS receive antenna gain patterns which includes the effects of satellite structures on their patterns. Fig. 2 depicts the antenna measurement setup. From an antenna range perspective, the GPS satellite antenna can be viewed as the illuminating source and the CYGNSS antenna, as the antenna under test (AUT). By reciprocity, the GPS satellite antenna can also be viewed as the AUT if the CYGNSS antenna pattern is known. Several sources have reported bounds on that the cross-pol (LHCP) component of the GPS satellites antennas as -15 dB or less. Indeed, the official GPS ICD specifies a cross-pol axial ratio value of less than ~1 dB [14]. Consequently, for this work, it is assumed that the GPS satellite antenna is purely RHCP. Although the CYGNSS zenith receive antenna is expected to have a significant LHCP pattern component (as shown in Section V.B), it is only the RHCP component that is expected to be measured using our approach. While any LHCP component of the GPS transmitted signal is expected to be small and not significant, if that is in fact not the case, then the derived CYGNSS receive antenna patterns presented here should not be viewed as pure RHCP patterns but rather as composite polarization patterns.

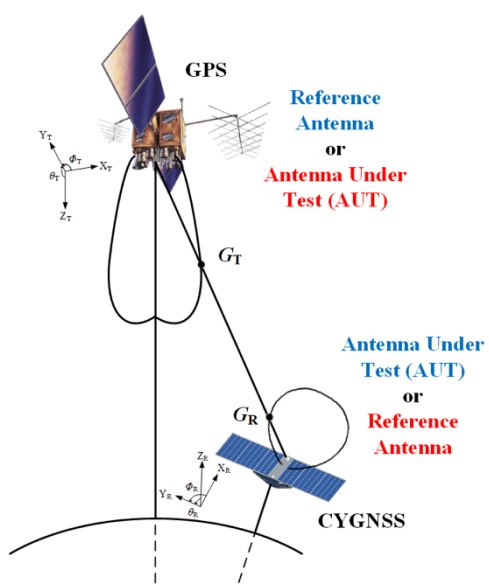

Fig. 2. Spaceborne antenna range measurement system formed by constellations of GPS and CYGNSS satellites (Note: not to scale)

C. Angular Sampling of the GPS Satellite Antenna Pattern

The use of the orbiting CYGNSS receivers is an attractive alternative to ground stations when it comes to achieving robust angular sampling of the GPS satellite antenna pattern. If we assume the GPS satellite attitude has a fixed yaw angle relative to its orbit coordinate frame, then the angular sampling of a single fixed ground station would be very limited. Reconstructing the GPS antenna pattern using a global GPS receiver network [23] is feasible, but it may require additional efforts in system calibration and signal processing. The highly repeatable 12-hour GPS orbit results in measurements made at a fixed ground location that cut through nearly identical slices of the GPS pattern day-after-day and month-after-month. This is illustrated in Fig. 3(a), which shows the location in the GPS antenna coordinate system of all samples made by a ground-based receiver over a 100-day period. In the figure, the radial coordinate is the angular distance from the antenna boresight and the azimuthal coordinate is the azimuthal angle about the boresight direction, with 0° referenced to the +X axis in the GPS satellite reference frame. A more detailed description of the coordinate system can be found in [15]. For the results shown in Fig. 3(a), the receiver was located in Ann Arbor, MI and the GPS satellite is SVN (space vehicle number) 54, but the results are similar for any fixed location and specific SV. It should be noted, however, that the GPS satellites are known to regularly adjust their yaw state in relation to the sun [24]. While this yaw information is not publicly available, such variations could result in an improved angular sampling of the GPS antenna pattern beyond that illustrated here. Nonetheless, the variation would still be less than if the receiver were instead located on a LEO satellite.

Compared to using a ground-based receiver to calibrate GNSS antennas, there is a distinct advantage in angular sampling when using a spaceborne receiver [25]. Fig. 3(b) shows the location of all samples made of a single GPS antenna pattern (in the GPS antenna coordinate system) by the 8 CYGNSS satellites in one day, and Fig. 3(c) shows the sampling distribution after 1 week. The GPS pattern is much more fully sampled by the CYGNSS satellites in one week than the ground-based system was able to in 100 days. For the work presented here, we use approximately 2 years of samples by the constellation of CYGNSS satellites for even better pattern coverage. The spaceborne antenna range system provides nearly gap-free measurements of the GPS satellite antenna pattern over all azimuth angles and out to an off-boresight angle of ~15.2 deg. The Earth horizon is located at ~13.8 deg in the GPS satellite antenna coordinate system and CYGNSS is able to measure the GPS satellite transmit gain pattern as it extends into the LEO space service volume due to its 520 km orbit altitude.

D. Sampling Density of GPS Satellite and CYGNSS Satellite Antenna Patterns

In this work, antenna patterns are estimated using measurements made by the spaceborne antenna range over a long time interval, to further improve the sampling distribution, to allow for detection of outlier data samples, and to average out the effects of measurement noise. Both GPS and CYGNSS antennas are jointly estimated, and they can each be treated as the AUT at different stages of the analysis.

Fig. 4 shows the sampling density for a particular GPS satellite antenna from 2018 DOY (day of year) 213 to 2020 DOY 182 using measurements from all 8 CYGNSS satellites. The sampling density is shown in the GPS satellite antenna coordinate system, and it accounts for the orientation of the GPS satellite. Changes in GPS yaw state [24] [26] are accounted for using the GIPSY-X (GNSS-Inferred Positioning System-X) software [27] licensed by NASA Jet Propulsion Laboratory (JPL). In the figure, the

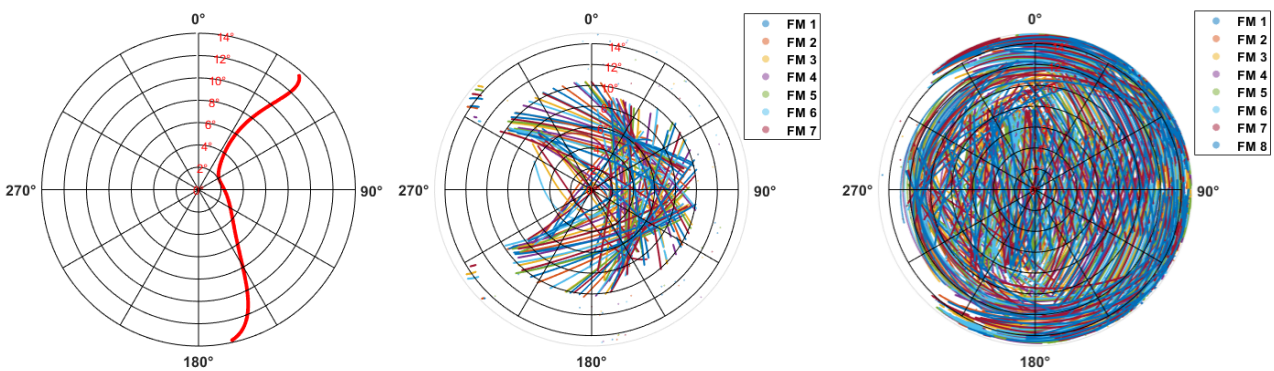

(a) (b) (c)

Fig. 3. Location in the GPS transmit antenna coordinate system of gain pattern measurements made by: (a) a ground-based receiver over 100 days; (b) 8 CYGNSS satellites in one day; (c) 8 CYGNSS satellites in 1 week. Note: These plots are based on data without GPS yaw correction

angular resolution of sampling density is 0.5×0.5 deg and the color map denotes the number of samples in each bin.

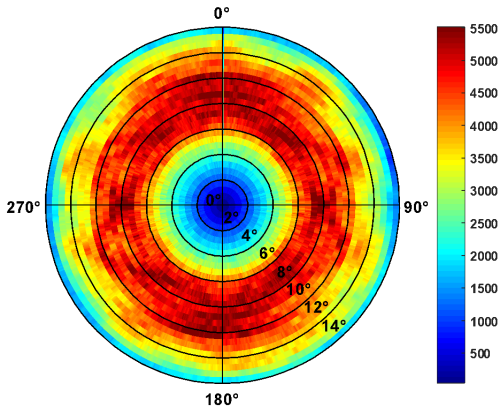

Fig. 4. Sampling density over GPS satellite's transmit antenna pattern using approximately 2 years of data

Fig. 5 shows the sampling density of a single CYGNSS antenna pattern in its coordinate system, using all data from the same time period as Fig. 4. Measurements in this figure are accumulated over a subset of GPS SVNs: 41, 43, 44, 45, 46, 51, and 56. This particular subset of GPS SVs is used because: 1) they correspond to older block types which have been found to exhibit less variability in their transmit power level than the more recent block types [28-30]; and 2) their antenna pattern have less azimuthal variability, according to the published patterns in [15]. The angular resolution in Fig. 5 and in the estimated CYGNSS antenna patterns is 1×1 deg.

The distribution of samples of the CYGNSS patterns is much less uniform than that of the GPS patterns. Samples are concentrated in the vicinity of azimuthal angles 90 and 270 deg, which correspond to the starboard and port directions relative to the forward motion of the CYGNSS satellites. This uneven sampling density results from a property of the CYGNSS GPS receivers, which records signals from GPS transmitters for which the signal reflected from the Earth surface enters the nadir science antenna in its main beam. The science antennas are fan beams pointed in the spacecraft's starboard and port directions. Only measurements of direct signals received by the zenith antenna that correspond to reflected signals received by the nadir antennas are downlinked to the ground. This restriction on the distribution of samples of the zenith pattern means that, unlike with the GPS patterns, its gain cannot be determined uniformly across the entire main beam. Fortuitously, it is only in the portions of the main beam that are well sampled that accurate antenna gain knowledge is required for purposes of CYGNSS science data calibration.

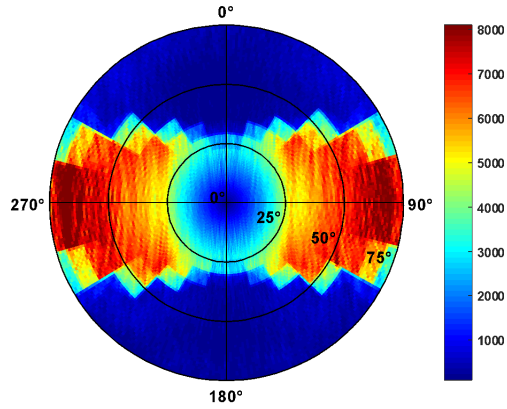

Fig. 5. Sampling density over CYGNSS satellite's receive antenna pattern using approximately 2 years of data

E. Equations for On-Orbit Received Power

The received power referenced to the output port of the CYGNSS zenith antenna, P_R, can be determined from P_Z, the calibrated power at the input port of the receiver, by correcting for the gain of the zenith low noise amplifier (LNA), G_{LNA}, according to

$$P_R = \frac{P_Z}{G_{LNA}(T_{LNA})} \tag{1}$$

where T_{LNA} is the temperature of the zenith LNA. G_{LNA} is calculated using a pre-launch look-up table (LUT) of gain vs. physical temperature. P_Z is converted from raw counts to power in watts based on the hardware calibration experiment described in our previous studies [10, 11].

The Friis transmission equation expresses the relationship between the received power and the gain of the transmit and receive antennas according to

$$P_R = \frac{\lambda^2}{(4\pi R)^2} P_T G_T(\theta_T, \phi_T) G_R(\theta_R, \phi_R) \tag{2a}$$

$$G_R(\theta_T, \phi_T) = \frac{(4\pi R)^2}{\lambda^2} \frac{P_R}{P_T G_T(\theta_T, \phi_T)} \tag{2b}$$

$$G_T(\theta_T, \phi_T) = \frac{(4\pi R)^2}{\lambda^2} \frac{P_R}{P_T G_R(\theta_R, \phi_R)} \tag{2c}$$

where G_T is the gain of the GPS transmit antenna, G_R is the gain of the zenith receiver antenna, R is the distance from the transmitter to the receiver, λ is the wavelength for GPS L1 signals, and P_T is the transmit power of the GPS satellite, θ_T is the GPS off-boresight angle from the nadir $(+Z_T)$, ϕ_T is the GPS azimuthal angle that is counter-clockwise around the boresight referenced to the $+X_T$ axis, θ_R is the CYGNSS off-boresight angle from its boresight $(+Z_R)$, and ϕ_R is the CYGNSS azimuthal angle that is counter-clockwise around the boresight referenced to the $+X_R$ axis, as depicted in the coordinate systems in Fig. 2.

Eq. (2b) and (2c) are used to compute the gain of the GPS

transmit antenna and CYGNSS receive antenna in the following sections.

III. ESTIMATION OF CYGNSS AND GPS SATELLITE ANTENNA PATTERNS

Either the GPS or the CYGNSS antenna can be considered the AUT. Depending on which one it is, one or the other of eqns. (2b) or (2c) is used to estimate the gain. Therefore, the estimation of one of the gain patterns presupposes knowledge of the other one. Both patterns can be estimated sequentially. The CYGNSS receive pattern, G_R, is estimated first by assuming that the published pre-launch GPS pattern is G_T. Next, the GPS pattern is estimated by assuming that the CYGNSS pattern is the G_R that was just determined. If the new GPS pattern is identical to the pre-launch pattern, then the estimation process is complete. As will be shown below, this turns out not to be the case, and an iterative procedure is developed instead which can jointly estimate both patterns.

A. Estimation of CYGNSS Zenith Antenna Patterns

There are eight CYGNSS spacecraft, which are designated flight model (FM) 1 to 8. Although all spacecraft and GPS antennas are meant to be identical, small differences in each antenna combined with differences in the deployment of satellite solar panels results in significant gain pattern differences. For this reason, each receive antenna pattern is determined independently. For each one, the pattern can be estimated using many different GPS SVs as the transmitter. We use the subset of seven GPS SVs noted above, because their transmit power level P_T is most stable over time. Examples of the resulting G_R patterns for FM 1 using SVN 43 and 46 are shown in Fig. 6(a) and 6(b), respectively. Several characteristics of the two patterns are noteworthy. Both are well sampled over the azimuthal ranges 75-105 deg and 255-285 deg for reasons discussed above. The two gain patterns are generally consistent in these two sectors. Outside of the sectors, the sampling density varies due to differences in the individual orbits of the GPS satellites and some angular regions are sampled better by one SV than the other. For this reason, it is desirable to combine together patterns estimated using multiple SVs to create a single, well-sampled composite pattern. Before doing so, it is prudent to test whether the patterns are consistent with one another within the angular region in which they overlap.

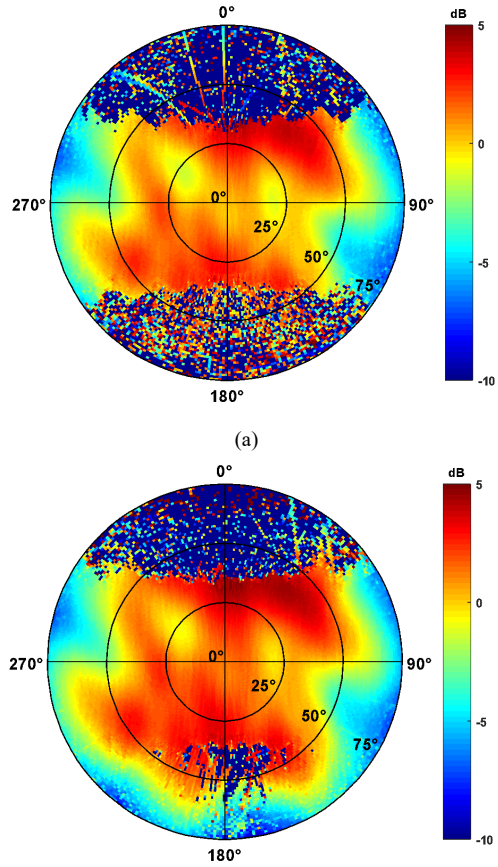

Fig. 6. Example of the retrieved zenith antenna gain pattern (FM 1) using signals from (a) GPS SVN 46 and (b) SVN 43

The average value of G_R over the two well-sampled sectors is considered individually for each FM derived from each SV. This value, referred to as the normalized integrated gain, G_{NI}, is given by

$$G_{NI} = \sum_{\theta_i=25}^{70} \left[\sum_{\phi_i=75}^{105} G_R(\theta_i, \phi_i) \sin\theta_i + \sum_{\phi_i=255}^{285} G_R(\theta_i, \phi_i) \sin\theta_i \right] \Delta\theta\Delta\phi \quad (3)$$

where θ_i and ϕ_i are the off-boresight and azimuthal angles and the discretized average is computed over ϕ_i within ± 15 deg of the port and starboard directions and over θ_i within 25-70 deg. $\Delta\theta$ and $\Delta\phi$ are the resolution over off-boresight and azimuth. These are the two sectors with consistently high sampling density for all SVs. N is the total number of pixels used.

A comparison of G_{NI} for the eight CYGNSS FMs and 7 GPS SVs is shown in Fig. 7(a). The different colors indicate different FMs and the x-axis is the GPS SVN. A shift in the average gain is evident between SVs that is consistent across all FMs. The most likely cause of the shift is errors in the assumed GPS transmit power levels of the

individual SVs. The values used for P_T are based on previous measurements made by a ground-based GPS power monitor system, as reported in [17, 18]. The shifts in G_{NI} for a fixed FM as SVN is varied represent differences in the error in P_T. It is not possible with this analysis to determine absolute values for each P_T, but it is possible to adjust their individual values so that any remaining error is common to all seven SVs. This is done by assuming the average value of P_T across all seven SVs is correct and then rescaling the individual values so that G_{NI} is consistent. The result is shown in Fig. 7(b), which is computed in the same way as Fig. 6(a) after the individual values of P_T have been adjusted. Once the P_T adjustment has been made, the individual G_R patterns derived from each SV can now be combined together into a single pattern. The result is shown in Fig. 8 for FM 1, where the center is the boresight and circles represent different off-boresight angles. Similar G_R patterns are computed in the same way for each FM.

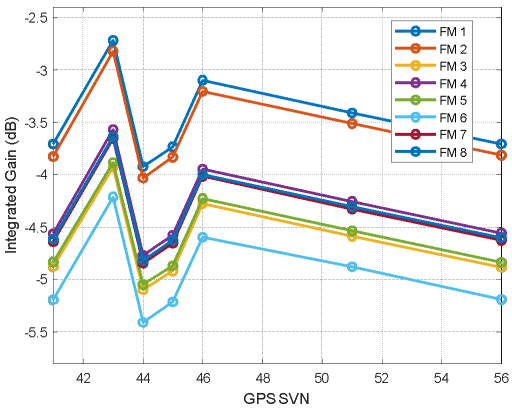

(a)

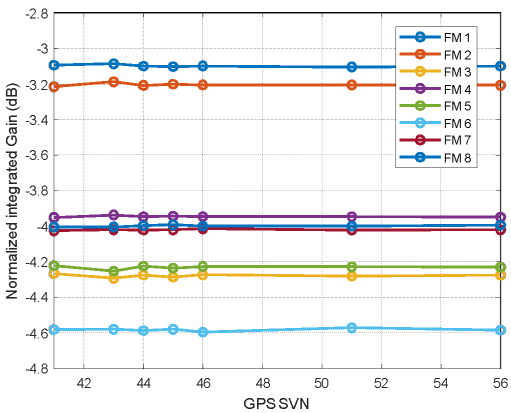

(b)

Fig. 7. Normalized integrated gain G_{NI} vs. GPS SVN for 8 FMs: (a) raw calculation; (b) bias removed

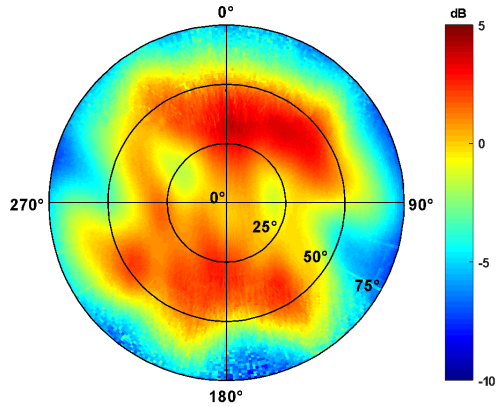

Fig. 8. Example of the retrieved zenith gain pattern (FM 1) using 7 SVs

B. Estimation of GPS Satellite Antenna Patterns

The antenna gain pattern G_T for GPS satellites can be estimated using (2c), when the eight FM patterns derived in the previous subsection are assumed for G_R. Similarly, G_T is retrieved using individual FM's measurements, as the examples given in Fig. 9 (a) and (b). The retrieved patterns of SVN 56 using measurements made by FM 1 and FM 2 are generally similar, while existing minor differences. This further confirms the correctness of the normalization process in previous subsection.

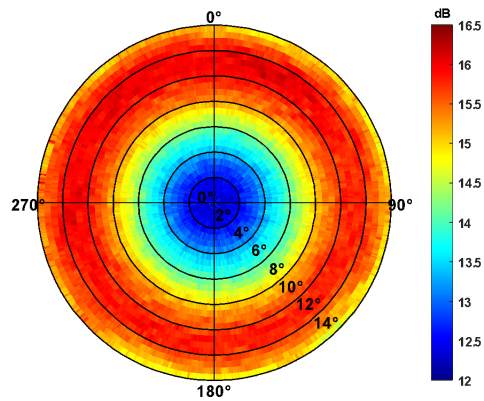

(a)

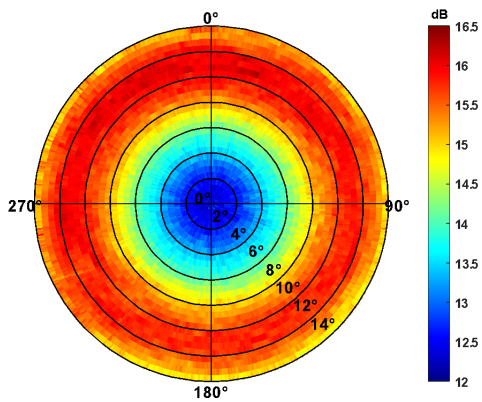

(b)

Fig. 9. Example of the retrieved GPS gain pattern (SVN 56) using signals from (a) CYGNSS FM 1 and (b) FM 2

Then the GPS antenna patterns retrieved from eight FMs' measurements are combined together by a weighting average to estimate the final pattern, as the example of SVN 56 shown in Fig. 10. The computed GPS antenna pattern is considered reliable at off-boresight angles of less than 12 deg. Above this angle, the low gain of the CYGNSS receive antenna reduces the received signal strength significantly.

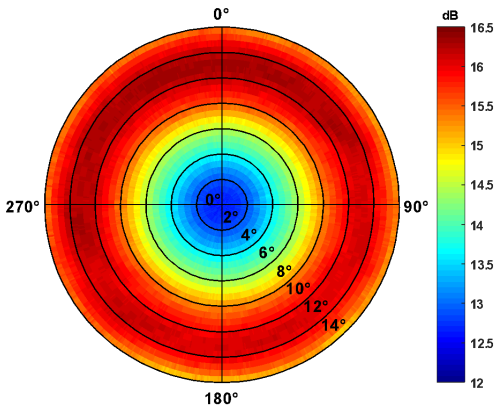

Fig. 10. Example of the retrieved GPS gain pattern (SVN 56) using signals from all eight CYGNSS FMs

IV. VALIDATION

A. CYGNSS Zenith Antenna Pattern

In order to provide validation of our measured CYGNSS zenith antenna pattern, anechoic chamber measurements were performed. Measurements took place in a compact antenna measurement test range at The Ohio State University ElectroScience Laboratory, as shown in Fig. 11. For these measurements, the antenna was mounted on an approximate CYGNSS satellite mock-up. These measured patterns are referred to as the pre-launch patterns. Dual-polarized measurements were made. The RHCP component is used for validation, while the LHCP component is included to provide additional information to the reader. Additional tests using different configurations were performed, and the results indicate that the platform has a significant effect on the CYGNSS antenna gain pattern. Therefore, considering the differences between the flight model and test model, as well as the disparities among the flight antennas, these chamber measurements alone should not be used for science calibration but should be improved upon with on-orbit measurements.

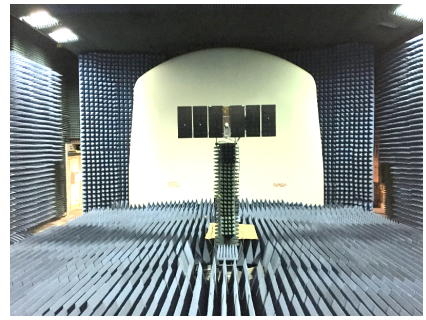

(a)

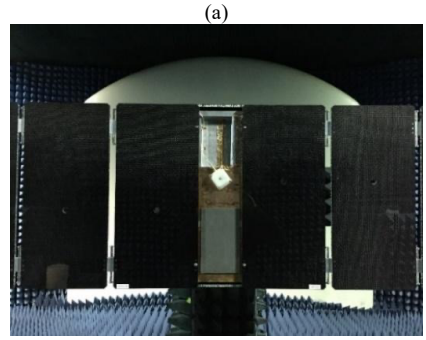

(b)

Fig. 11. (a) Compact range measurement of the CYGNSS zenith antenna. (b) a close-up view of the antenna (small white square) on the approximate satellite mock-up

Fig. 12 shows the pre-launch measured pattern of the CYGNSS antenna mounted on a spacecraft mock-up. Note that the pre-launch measured pattern is re-scaled to remove a calibration offset (2.5 dB), which is believed to originate from the GPS receiver instrument aboard the satellite. It is clear that the pre-launch and retrieved pattern in Fig. 8 are qualitatively very similar, which gives us confidence about the accuracy of the pattern estimation method in general. However, there are significant differences between them as well. It should be noted that the CYGNSS zenith antenna is a miniatured, single-layer patch antenna, which we would expect to have a smooth and uniform pattern. However, on the spacecraft, the antenna is mounted in a narrow channel between the edges of the large solar panels that results in significant near-field coupling of the antenna, platform multipath, and detuning of the patch. These effects are evident in the rapid variations in the measured antenna pattern in Fig. 12 as well as in its striking pattern asymmetry. In this configuration, the pattern of the antenna is very sensitive to small variations in the satellite structure or in manufacturing differences between different antennas. Thus, we expect there to be significant differences between the pre-launch measurements on the approximate satellite mock-up and the on-orbit measurements using the real satellite platforms. These differences support the notion that antenna patterns should be independently determined for each of the CYGNSS spacecraft while on-orbit in their operational environment and is the primary motivation for this work.

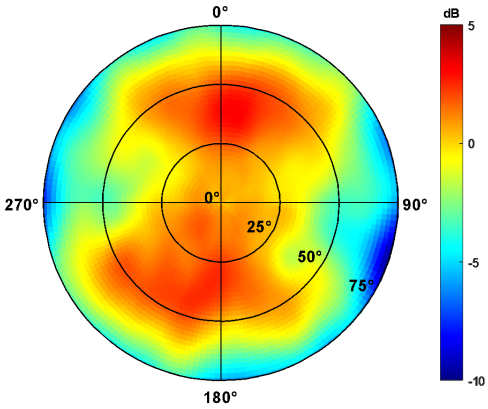

Fig. 12. Scaled pre-launch measured pattern using a satellite mock-up

The cross-polarization isolation of the pre-launch CYGNSS antenna pattern measurements is shown in Fig. 13. This is the difference (in dB) between the RHCP and LHCP pattern components. The observed cross-pol isolation is quite poor, with most angles being between 6-12 dB and some angles being as little as 3 dB. It is expected that this is due to the effects of the coupling and scattering of the satellite platform on the otherwise well-designed patch antenna. If one focuses on angles with the highest measurement density (Fig. 5), one can interpret the average cross-pol isolation as being approximately 10 dB over the set of measurements used to estimate the GPS satellite antenna patterns. Nonetheless, as mentioned earlier, since the GPS satellite transmit antenna has been reported as having a cross-polarization isolation of more than 20dB, we can conclude that the on-orbit approach is measuring the RHCP components of both the transmit and in-situ receive antenna patterns (that is, the receive antenna pattern that incorporates all effects of the receiver satellite platform).

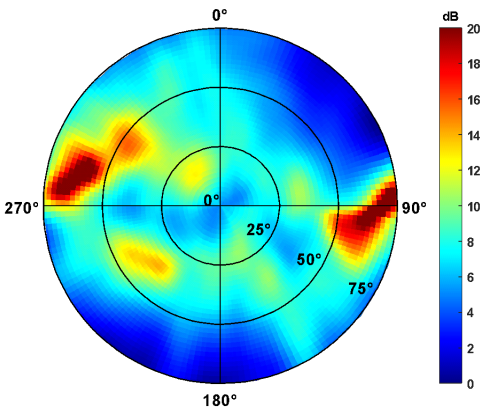

Fig. 13. Measured cross-polarization isolation (dB) for pre-launch patterns with a satellite mock-up

B. GPS Satellite Antenna Gain Pattern

Fig. 14 shows the published pre-launch pattern for GPS SVN 56 published in [15]. The retrieved pattern in Fig. 10 shows azimuthal asymmetry features which are generally consistent with those of the pre-launch pattern. However, because of its much higher angular resolution, small features can be seen in the retrieved pattern that cannot be resolved by the pre-launch one.

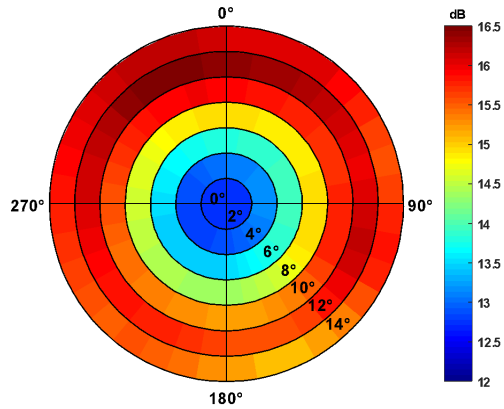

Fig. 14. Published GPS antenna patterns of SVN 56 [15]

Fig. 15 plots the difference between the pre-launch G_T pattern and the one derived here. Note that the published pre-launch patterns are only available with a coarse 2×10 deg resolution so the retrieved pattern has been smoothed to that same resolution to compute the difference. It shows clear signs of structural differences between the two antenna patterns, as opposed to unstructured, random differences that might be attributed to measurement noise. To minimize uncertainty in antenna patterns, an iterative solution is being considered next which updates estimates of G_R and G_T at each iteration. The objective is for the iterative process to converge to a pair of patterns that are mutually consistent with the measured values of P_R, as stipulated by the relationship in (3). This will be studied as our future work.

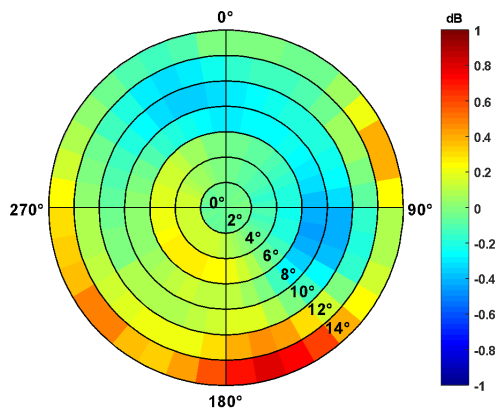

Fig. 15. Difference between the published pre-launch pattern and the retrieved pattern for SVN 56

V. DISCUSSION

A. Summary of Results

Table II summarizes the limited knowledge of the GPS and CYGNSS antenna patterns prior to the work presented here, and the improvements that have been made. Specifically: 1) For CYGNSS antennas, 8 estimated gain patterns were characterized in their operational environment, compared with only 1 pre-launch measured pattern using a single, crude CYGNSS satellite mock-up; 2) For GPS antennas, more than 31 GPS patterns are estimated precisely (0.5×0.5 degrees) and accurately when the antennas are mounted on the satellites and in their operational environment, compared with only 20 published pre-launch measured patterns with rather coarse (2×10 deg) angular resolution.

TABLE II
IMPROVEMENT OF ANTENNA PATTERN CHARACTERIZATION

Antenna	Before	After
GPS	20 pre-launch measured patterns with limited angular resolution (2×10 degrees)	>31 estimated patterns with antenna in its operational environment (0.5×0.5 degrees)
CYGNSS	1 pre-launch measured pattern using a spacecraft mock-up	8 estimated patterns in its operational environment

Note that the two sets of antenna patterns need to be validated with independent measurement, e.g. received signals observed by calibrated ground-based GNSS systems or other spaceborne GNSS receivers.

B. Impact on CYGNSS Level 1 Calibration

These antenna gain patterns have been applied to the official version 3.0, 3.1, and 3.2 Level 1 calibration and science data processing algorithms of the NASA CYGNSS mission, specifically on the dynamic EIRP calibration approach descripted in [11]. The CYGNSS zenith antenna gain patterns are used to calibrate the CYGNSS direct signal and to estimate the GPS EIRP in the direction of the CYGNSS spacecraft E_Z. Then the GPS EIRP in the direction of the specular reflection point E_S is estimated by using the zenith-to-specular ratio (ZSR) functions, which are derived from the retrieved GPS antenna gain patterns. E_S serves as a key input to the Level 1 calibration algorithm described in [8, 9].

Two independent approaches, root of sum of squares (RSS) analysis and Monte Carlo simulation, are used for error analysis, and they agree well with both estimating ~0.32-dB relative error. This reduces the 0.4-dB error term of GPS EIRP in v2.1 Level 1 calibration [9] by approximately 20%. Besides, the 0.4-dB error does not consider flex power events which can introduce greater than 2-dB errors due to the variation of GPS transmit power, thus the improvement could be significantly larger.

The dynamic EIRP calibration algorithm has been proved to be able to instantaneously detect and correct for power fluctuations in all GPS transmitters and significantly reduces errors due to the azimuthal asymmetry of the GPS antenna gain patterns. It allows observations with Block IIF transmitters (approximately 37% of the entire data set) to be included in the standard data products and further improves the calibration quality [11].

VI. SUMMARY AND FUTURE WORK

This paper presents an approach that estimates RHCP gain patterns of GPS satellite and CYGNSS antennas using spaceborne measurement. Actual on-orbit data are used to determine the patterns in their operational environment. This cannot be practically achieved prior to launch using ground-based systems. A high-resolution map of the complete on-Earth portion of the GPS satellite antenna's main beam results. The new GPS and CYGNSS patterns have been incorporated into the science data processing algorithms used by the CYGNSS mission and have resulted in improved calibration performance [11].

Future work will focus on: 1) revisiting the end-to-end zenith calibration experiment; 2) identifying calibration error sources including: a) time variations of the GPS transmit power; b) aging of the CYGNSS receiver system, which could introduce time-dependent errors in calibration of the received power, P_R; c) radio frequency interference (RFI) in the CYGNSS received signal (also possibly time dependent); 3) making appropriate empirical corrections and quality control to received signals; 4) developing an iterative retrieval process to minimize retrieval uncertainty; 5) analyzing the systematic differences between retrieved antenna patterns; 6) performing absolute calibration and error analysis of antenna patterns for all GPS transmitters; and 7) validating the retrieved patterns with independent measurements.

ACKNOWLEDGMENT

The work presented here was supported in part by NASA Science Mission Directorate contract NNL13AQ00C with the University of Michigan.

The authors would like to thank the editor and reviewers for their insightful and invaluable comments towards improving our manuscript.

REFERENCES

[1] B. Hofmann-Wellenhof, H. Lichtenegger, and J. Collins, *Global Positioning System: Theory and*

Practice, 5th ed. Vienna, Austria: Springer-Verlag, 2001.

[2] P.Misra and P. Enge, *Global Positioning System: Signals, Measurements, and Performance*, 2nd ed. Lincoln, MA, USA: Ganga-Jamuna Press, 2001.

[3] V. U. Zavorotny, S. Gleason, E. Cardellach, and A. Camps, "Tutorial on remote sensing using GNSS bistatic radar of opportunity," *IEEE Geosci. Remote Sens. Mag.*, vol. 2, no. 4, pp. 8-45, Dec. 2014.

[4] S. Gleason, S. Lowe, and V. Zavorotny, "Remote sensing with bistatic GNSS reflections," in *GNSS Applications and Methods*, S. Gleason and D. Gebre-Egziabher, Eds. Boston, MA, USA: Artech House, 2009, pp. 399-436.

[5] S. Gleason, "Remote sensing of ocean, ice and land surfaces using bistatically scattered GNSS signals from low earth orbit," Ph.D. dissertation, Dept. Appl. Phys., Univ. Surrey, Guildford, U.K., 2006.

[6] C. S. Ruf, S. Gleason, Z. Jelenak, S. Katzberg, A. Ridley, R. Rose, J. Scherrer, and V. Zavorotny, "The CYGNSS nanosatellite constellation hurricane mission," in *Proc. IEEE Int. Geosci. Remote Sens. (IGARSS)*, Munich, Germany, Jul. 2012, pp. 214-216.

[7] C. Ruf, M. Unwin, J. Dickinson, R. Rose, D. Rose, M. Vincent, and A. Lyons, "CYGNSS: Enabling the future of hurricane prediction," *IEEE Geosci. Remote Sens. Mag.*, vol. 1, no. 2, pp. 52-67, June 2013.

[8] S. Gleason, C. S. Ruf, M. P. Clarizia, and A. J. O'Brien, "Calibration and unwrapping of the normalized scattering cross section for the cyclone global navigation satellite system," *IEEE Trans. Geosci. Remote Sens.*, vol. 54, no. 5, pp. 2495-2509, May 2016.

[9] S. Gleason, C. S. Ruf, A. J. Orbrien, and D. S. McKague, "The CYGNSS Level 1 calibration algorithm and error analysis based on on-orbit measurements," *IEEE J. Sel. Topics Appl. Earth Observ. Remote Sens.*, vol. 12, no. 1, pp. 37-49, Jan. 2019.

[10] T. Wang, C. Ruf, S. Gleason, B. Block, D. McKague, and A. O'Brien, "A real-time EIRP Level 1 calibration algorithm for the CYGNSS mission using the zenith measurements," in *Proc. IEEE Int. Geosci. Remote Sens. Symp. (IGARSS)*, Yokohama, Japan, 2019, pp. 8725-8728.

[11] T. Wang, C. Ruf, S. Gleason, A. O'Brien, D. McKague, B. Block, and A. Russel, "Dynamic calibration of GPS effective isotropic radiated power for GNSS-reflectometry Earth remote sensing," *IEEE Trans. Geosci. Remote Sens.*, vol. 60, pp. 1-12, 2022.

[12] F. M. Czopek and S. Shollenberger, "Description and performance of the GPS Block I and II L-Band antenna and link budget," in *Proc. 6th Int. Tech. Meeting Satell. Division Inst. Navigat. (ION GNSS+)*, Salt Lake City, UT, USA, Sept. 1993, pp. 37-43.

[13] M. C. Moreau, F. H. Bauer, J. Russell Carpenter, E. P. Davis, G. W. Davis, and L. A. Jackson, "Preliminary results of the GPS flight experiment on the high Earth orbit AMSAT-OSCAR 40 spacecraft," in *Proc. 25th Annual American Astronautical Society Guidance and Control Conference*, Breckenridge, CO, USA, Feb. 2002, pp. AAS-02-004.

[14] GPS Technical References, Online: https://www .navcen.uscg.gov/gps-technical-references.

[15] W. A. Marquis and D. L. Reigh, "The GPS block IIR and IIR-M broadcast L-band antenna panel: Its pattern and performance," Navigat., J. Inst. Navigat., vol. 62, no. 4, pp. 329–347, Winter 2015.

[16] P. Steigenberger, S. Thoelert, and O. Montenbruck, "GNSS satellite transmit power and its impact on orbit determination," *J. Geodesy*, vol. 92, no. 6, pp. 609-624, June 2018.

[17] T. Wang, C. Ruf, S. Gleason, B. Block, D. McKague and D. Provost, "Development of GPS constellation power monitor system for high accuracy calibration/validation of the CYGNSS L1B data," in *Proc. IEEE Int. Geosci. Remote Sens. Symp. (IGARSS)*, Fort Worth, TX, USA, 2017, pp. 1008-1011.

[18] T. Wang, C. S. Ruf, B. Block, D. S. McKague, and S. Gleason, "Design and performance of a GPS constellation power monitor system for improved CYGNSS L1b calibration," *IEEE J. Sel. Topics Appl. Earth Observ. Remote Sens.*, vol. 12, no. 1, pp. 26-36, Jan. 2019.

[19] T. Wang, C. Ruf, B. Block, and D. McKague, "Characterization of the transmit power and antenna pattern of the GPS constellation for the CYGNSS mission," in *Proc. IEEE Int. Geosci. Remote Sens. Symp. (IGARSS)*, Valencia, Spain, 2018, pp. 4011-4014.

[20] J. E. Donaldson, J. J. K. Parker, M. C. Moreau, D. E. Highsmith, and P. D. Martzen, "Characterization of on-orbit GPS transmit antenna patterns for space users," *Navigat., J. Inst. Navigat.*, vol. 67, no. 2, pp. 411-438, 2020.

[21] T. Wang, "Engineering calibration and physical principles of GNSS-reflectometry for Earth remote sensing," Ph.D. dissertation, University of Michigan, Ann Arbor, MI, 2021.

[22] A. Camps, H. Park, G. Foti and C. Gommenginger, "Ionospheric effects in GNSS-Reflectometry from space," in *IEEE Journal of Selected Topics in Applied Earth Observations and Remote Sensing*, vol. 9, no. 12, pp. 5851-5861, Dec. 2016.

[23] G. Allende-Alba, S. Thoelert, and S. Caizzone, "Gain pattern reconstruction of GPS satellite antennas using a global receiver network", vol. 69, no. 3, 2022.

[24] Y. E. Bar-Sever, "A new model for GPS yaw attitude," *J. Geodesy*, vol. 70, pp. 714-723, Nov. 1996.

[25] T. Wang, C. Ruf, B. Block, D. McKague, and S. Gleason, "Characterization of GPS L1 EIRP: Transmit power and antenna gain pattern," in *Proc. 31st Int. Tech. Meeting Satell. Division Inst. Navigat. (ION GNSS+)*, Miami, FL, USA, 2018, pp. 2879-2890.

[26] J. Kouba, "A simplified yaw-attitude model for

eclipsing GPS satellites," *GPS Solutions*, vol. 13, no. 1, pp. 1-12, 2009.

[27] S. Desai *et al*. *GNSS-inferred positioning system and orbit analysis simulation software (GYPSY-OASIS)*. Internet. Accessed: Jan. 2018. [Online]. Available: https://gipsy-oasis.jpl.nasa.gov/.

[28] P. Steigenberger, A. Hauschild, S. Thoelert, and R. B. Langley, "US air force puts more power into GPS block IIR-M C/A-code," *GPS World*, vol. 28, no. 4, pp. 8-9, Apr. 2017.

[29] S. Thoelert, A. Hauschild, P. Steigenberger, R. B. Langley, and F. Antreich, "GPS IIR-M L1 transmit power redistribution: Analysis of GNSS receiver and high-gain antenna data," *Navigat., J. Inst. Navigat.*, vol. 65, no. 3, pp. 423-430, 2018.

[30] P. Steigenberger, S. Thoelert, and O. Montenbruck, "Flex power on GPS Block IIR-M and IIF," *GPS Solutions*, vol. 23, no. 1, pp. 1-12, 2019.

Tianlin Wang (Member, IEEE) received the B.E. degree in electrical engineering from the East China University of Science and Technology, Shanghai, China, in 2009, the M.S. degree in radio physics from Fudan University, Shanghai, China, in 2012, and the Ph.D. degree in electrical engineering from the University of Michigan, Ann Arbor, MI, USA, in 2021.

He is currently a President's Postdoctoral Scholar in the Department of Electrical and Computer Engineering and ElectroScience Laboratory of The Ohio State University. His research interests include wave propagation and scattering, microwave remote sensing, microwave measurements, and radio frequency (RF) circuits.

Dr. Wang is a member of Tau Beta Pi, Eta Kappa Nu, American Geophysical Union, and Institute of Navigation and an Early Career Member of Commission F of the U.S. National Committee for the Union Radio Scientifique Internationale. He received the 2018 IEEE Mikio Takagi Student Prize, an Outstanding Student Presentation Award at the 2018 AGU Fall Meeting, the 2020 Richard F. and Eleanor A. Towner Prize for Distinguished Academic Achievement and Distinguished Leadership Award from the University of Michigan, and the 2021 Ernest K. Smith USNC-URSI Student Prize. He is a recipient of the 2020 President's Postdoctoral Scholars Program (PPSP) Fellowship from The Ohio State University and the 2021 Mistletoe Research Fellowship from the Momental Foundation. He is currently serving as a co-chair of the IEEE Geoscience and Remote Sensing Society (GRSS) Modeling in Remote Sensing Technical Committee, a member of the GRSS Chapters Committee, and a member of the GRSS Young Professionals (YP) Committee.

Christopher S. Ruf (Life Fellow, IEEE) received the B.A. degree in physics from Reed College, Portland, OR, USA, in 1982, and the Ph.D. degree in electrical and computer engineering from the University of Massachusetts at Amherst, Amherst, MA, USA, in 1987.

He is the Frederick Bartman Collegiate Professor of climate and space science with the University of Michigan and Principal Investigator of the NASA Cyclone Global Navigation Satellite System Mission. He has worked previously at Intel Corporation, Hughes Space and Communication, the NASA Jet Propulsion Laboratory, Pasadena, CA, USA, and Penn State University, State College, PA, USA. His research interests include GNSS-R remote sensing, microwave radiometry, atmosphere and ocean geophysical retrieval algorithm development, and sensor technology development.

Dr. Ruf is a member of the American Geophysical Union, the American Meteorological Society, and Commission F of the Union Radio Scientifique Internationale. He was a recipient of the 1997 IEEE TGRS Best Paper Award, the 1999 IEEE Resnik Technical Field Award, the 2006 IGARSS Best Paper Award, the 2014 IEEE GRSS Outstanding Service Award, the 2017 AIAA SmallSat Mission of the Year Award, and the 2020 University of Michigan Distinguished Faculty Achievement Award. He is a former Editor-in-Chief of the IEEE TRANSACTIONS ON GEOSCIENCE AND REMOTE SENSING and has served on the editorial boards of Radio Science, the Journal of Atmospheric and Oceanic Technology, and Nature Scientific Reports.

Andrew J. O'Brien has worked in the area of adaptive GNSS antenna arrays and precision GNSS receiver algorithms for over a decade. He previously served as a Research Scientist with the ElectroScience Laboratory, Department of Electrical and Computer Engineering, The Ohio State University, Columbus, OH, USA. There, his primary research focused on spaceborne GNSS remote sensing using CYGNSS, TDS-1, and soil moisture active passive (SMAP). He served as a member of the CYGNSS Science Team and supported the development of CYGNSS end-to-end simulator and CYGNSS engineering activities. His other research activities included GNSS antenna arrays, antenna electronics, electromagnetic simulation, and radar systems.

Scott Gleason (Senior Member, IEEE) received the B.S. degree in electrical and computer engineering from the State University of New York at Buffalo, Buffalo, NY, USA, the M.S. degree in engineering from Stanford University, Stanford, CA, USA, and the Ph.D. degree in applied physics from the University of Surrey, Surrey, U.K., in 1991, 1999 and 2007, respectively. He is currently the President of the Daaxa LLC consulting company, specializing in GNSS instruments, calibration and remote sensing applications. He is a Co-Investigator on the science team and Instrument Scientist for the NASA CYGNSS mission. He has worked in the areas of astronautics, remote sensing and global navigation satellite systems for more than 20 years, including at NASAs Goddard Space Flight Center, Stanford's GPS Laboratory, Surrey Satellite Technology Limited, Concordia University (Montreal, Canada), Southwest Research Institute, the University Corporation for Atmospheric Research and the National Oceanography Centre, Southampton, U.K.

Darren S. McKague (Member, IEEE) received the Ph.D. degree in Astrophysical, Planetary, and Atmospheric Sciences from the University of Colorado, Boulder, in 2001. He is an Associate Research Scientist in the Department of Climate and Space Sciences and Engineering at the University of Michigan. Prior to working for Michigan, he worked as a systems engineer for Ball Aerospace and for Raytheon, and as a research scientist at Colorado State University. His work has focused on remote sensing with emphases on the development of space-borne microwave remote sensing hardware, microwave remote sensor calibration techniques, and on mathematical inversion techniques for geophysical retrievals. His experience with remote sensing hardware includes systems engineering for several advanced passive and active instrument concepts and the design of the calibration subsystem on the Global Precipitation Mission (GPM) Microwave Imager (GMI) as well as the development of calibration and inter-calibration techniques for the GPM constellation. His algorithm experience includes the development of a near-real time algorithm for the joint retrieval of water vapor profiles, temperature profiles, cloud liquid water path, and surface emissivity for the Advanced Microwave Sounding Unit (AMSU) at Colorado State University, and the development of the precipitation rate, precipitation type, sea ice, and sea surface wind direction algorithms for the risk reduction phase of the Conical scanning Microwave Imager/Sounder (CMIS).

Bruce P. Block received the B.S. degree in electrical engineering from the University of Michigan, Ann Arbor, MI, USA. He is a Lead Engineer in Research at the Space Physics Research Laboratory, College of Engineering, University of Michigan, where he developed hardware and software for ground testing of the CYGNSS Delay Doppler Mapping Instrument. In addition to his interests in Global Navigation Satellite System (GNSS) technology for geodesy and remote sensing, he has, over the course of 40 years, developed numerous electro-mechanical designs for spaceborne mass spectrometry, Langmuir probe, and gas chromatography instruments in collaboration with NASA's Goddard Space Flight Center, Jet Propulsion Laboratory, and Marshall Space Flight Center; JHU Applied Physics Laboratory; and the European Space Agency.

Anthony Russel received the B.S. degree in computer science engineering from Michigan State University, East Lansing, MI, USA, in 2014. He is a member of the engineering staff with the Space Physics Research Laboratory, College of Engineering, University of Michigan, Ann Arbor, MI, USA. His primary engineering activities involve algorithm development and large-scale data processing as a member of the Science Operations Center for the CYGNSS mission.